# WiCare: Towards In-Situ Breath Monitoring

Jin Zhang[1 2], Weitao Xu[3], Wen Hu[1 2], Salil S. Kanhere[1]
[1]The University of New South Wales, Australia
[2]CSIRO Digital Productivity Flagship, Australia
[3]The University of Queensland, Australia
jin.zhang1@unsw.edu.au,w.xu3@uq.edu.au,{wen.hu,salil.kanhere}@unsw.edu.au

## ABSTRACT

Respiratory conditions significantly impact the health of individuals in the modern society. Long-term breath monitoring is critical for diagnosing the onset of various chronic respiratory diseases. Traditional breathing monitoring methods rely on wearable devices (e.q. face masks or chest bands) which are intrusive and uncomfortable. Recent research has demonstrated that it is possible to use device-free WiFi sensing to monitor breathing. However, these approaches only work when the monitored individual is stationary, i.e., sleeping or sitting perfectly still. In this paper, we propose WiCare, a system that employs the off-the-shelf WiFi devices and is able to monitor *in-situ* breathing rate in a natural setting where the individual can perform actions such as reading, writing, using phone, etc, which we refer to as *micro motions*. WiCare exploits Channel State Information (CSI) of WiFi data and can effectively distinguish breathing from the micro motions performed by the monitored individuals. The key idea is that certain specific subcarriers carry strong imprints of breathing motions because of the multipath effect and frequency and spacial diversity of MIMO systems. We model breathing signals as periodical sinusoidal waves and use curve fitting realised by interior point non-linear optimisation to identify breath in time series of each subcarrier. The goodness of fit measured by Dynamic Time Warping is exploited to select subcarriers that effectively capture breathing. Indepedent component analysis is used to precisely isolate the breathing signals. We recruit five participants to perform 9 common micro motions. Our extensive experiments show WiCare can accurately distinguish breathing from the micro motions and estimate breath rate with an average accuracy of over 90%. WiCare also outperforms the state-of-the-art breath rate estimation methods by up to 80%. WiCare represents a first and important step towards *in-situ* breath monitoring in natural settings.

## CCS CONCEPTS

• **Human-centered computing** → *Ubiquitous and mobile computing*;

## KEYWORDS

channel state information (CSI); breath monitoring; multipath effect


*MobiQuitous 2017, November 7–10, 2017, Melbourne, VIC, Australia*

ACM ISBN 978-1-4503-5368-7/17/11…$15.00
https://doi.org/10.1145/3144457.3144467

## 1 INTRODUCTION

Respiratory conditions can significantly impact the health of individuals. According to WHO report [5], the top five respiratory diseases account for 17.4% of all deaths and 13.3% of all disability assisted life years, i.e., the numbers of years lost due to ill-health, disability or early death. In the modern society tobacco use, indoor and outdoor air pollution likely foster the growing rate of the chronic respiratory diseases (CRD) including asthma and lung cancer [22]. Monitoring the respiration profile of an individual is important for the early diagnosis of several illnesses such as pneumonia and congestive cardiac failure. Thus, an *in-situ* and cost-effective method for identifying respiratory conditions is highly desirable. Breathing rate (measured as the number of breaths per minute) is widely used as an indicator in regulatory health diagnoses [16].

The typical approach for measuring the breathing rate requires the subject to attach sensors such as accelerometer and pressure sensors on their body to detect the expansion and contraction of their chest incurred during the respiration process [2]. However, such methods are very intrusive and thus unsuitable for long term *in-situ* measurement. There has thus been an increasing interest in leveraging RF-based methods as an alternative for breath monitoring. The expansion and contraction of the chest during breathing creates unique perturbations in the radio spectrum which can be used to detect and subsequently measure the breathing rate. The measurements can be conducted in a passive and non-intrusive manner (i.e., without requiring the subject to wear any equipment) making this an attractive approach for long-term monitoring. A solution for measuring breathing rate is presented in [8], but it relies on specialised hardware (e.g., radar). On the other hand, WiFi signals are widely abundant in our personal spaces (homes, offices, etc). Recent research [19] [17] [18] [30] has demonstrated that by measuring the fluctuations in the WiFi signals which are revealed by analyzing the fine-grained Channel State Information (CSI), it is possible to monitor the breathing rate of an individual. While these works show great promise, they can only measure the breathing rate in a controlled environment where the subject must be stationary, i.e. either sleeping [19] or sitting still [24].

In this paper, we take a first step towards realising a system that can monitoring the breathing rate of an individual in a completely natural setting as they go about their daily activities. We consider a setting where the subject being monitored can perform certain *micro* motions while seated, i.e., engage in natural activities that involve movement of their head and/or arms but not their torso. Examples include reading a book, using a mobile device, typing

**Figure 1: Operational Scenario for WiCare**

on a keyboard, etc. (detailed list is in Table 1) which are typical activities performed by an individual while relaxing at home [20]. We exclude more *intense* motions that involve movement of the torso and legs, since the perturbations in the WiFi signals caused by these activities significantly overpower those induced by the minute chest motions during breathing.

We present WiCare, a WiFi based breath monitoring system that is deployed on commercial off-the-shelf WiFi devices. A transmitter node (any typical WiFi device) continuously sends packets to a receiver node, which passively records CSI data from the received packets as shown in Fig. 1. The CSI data captures the aggregate effect of multi-path, shadowing and interference on the WiFi signals in the given environment. The expansion and contraction of the chest during breathing impacts the environment in a unique way, which changes the effect of these phenomena on the WiFi signal. These in turn are manifested as unique perturbations in the CSI data, reflecting the breathing rate. However, the micro motions performed by the subject also influence the WiFi signal, albeit in a different manner. There are several significant challenges in separating the patterns caused by the breathing signals from those of the micro motions and ultimately achieve accurate breath monitoring, even in this seemingly simplified setting.

The first technical challenge is to identify the range of frequencies which are most influenced by breathing when the CSI data is transformed to the frequency domain using Continuous Wavelet Transformation (CWT). Using empirically collected data, we find that breathing impacts a much narrower range of frequencies as compared to the impact of micro motions which is more spread out. We extract signals from the former frequency range to mitigate the impact of micro motions. However, these frequencies are also influenced by micro motions. The extracted CSI data thus captures a significant part of the breath motions mixed with some parts of the micro motions.

The second challenge is to determine which subcarriers in the CSI data exclusively contain breath motions. In general, breathing signals can be modelled as periodic sinusoidal waves while micro motions as non-sinusoids. We compare the time series data of each subcarrier with a sinusoidal template to determine which subcarriers are most likely to contain the breath motions. We use curve fitting realised by interior point non-linear optimisation for this purpose. The goodness of the fit is measured by Dynamic Time Warping. The subcarriers with the best fit are selected for further processing.

The selected carriers capture pronounced chest motions but will also reflect the impact of the accompanying micro motions. The third challenge is to precisely isolate the breathing signals. The selected subcarrier data will now only contain two main sources of perturbations, i.e., breathing and micro-motions, of which the former is most dominant. Thus, we use Independent Component Analysis (ICA) to isolate the breathing signals. A peak detection method is used to estimate the breathing rate.

We conduct extensive experiments to evaluate the performance of WiCare using 5 subjects in a scenario consistent with Fig. 1. The subjects being monitored are asked to perform 9 different natural micro motions as outlined in Table 1. Our system can accurately estimate breath rate with an average accuracy of over 90%. We also show that WiCare can outperform the state-of-the-art breath rate estimation method [17] by up to 80%.

The remaining paper is organised as follows. Section 2 discusses the related work. Section 3 introduces the Channel State Information (CSI) and propagation model. Section 4 explains the whole WiCare system. Section 5 presents WiCare system design and evaluates the performance with extensive experiments. Section 6 concludes this paper.

## 2 RELATED WORK

Traditional approaches for breath monitoring rely on the use of body worn sensors. These approaches are intrusive and thus infeasible for long-term monitoring of individuals in their natural settings. Specifically, [4] uses nasal mask to monitor air flow for breath monitoring. The large size and obtrusive shape of the mask is inconvenient for the continuous long-term breath monitoring. Researchers in [2] [3] have embedded inertial measurement units (IMUs) in shirts for detecting chest motions induced by breathing. However, the IMU sensors must be tightly attached to the body, which makes long-term monitoring challenging.

The RF based contact free techniques are widely used for vital signs detection. Several studies have demonstrated the use of radar for breath monitoring including: doppler radar [11], frequency modulated continuous wave (FMCW) radar [6] and ultra wide band (UWB) pulse radar [37] [8]. However, all of the above require specialised hardware (i.e. radars) which may limit their wider applicability. In [21], the received signal strength (RSS) measurements collected by a wireless sensor network are used to detect breath. However the system requires a dense deployment of sensor nodes which is not scalable. The ubiquity of WiFi signals in our environments (home, office, public spaces, etc.) offers a cost-effective approach for implementing RF sensing. [33] utilises the WiFi signals to recognise the human activities including standing, sitting, walking and sleeping. WiFi-ID [36] leverages the fact that each individual has a unique gait which is manifested as a unique pattern in the WiFi signals to uniquely identify that individual. [28] [29] focus on hand and finger gesture recognition.

Recent works also exploit WiFi signals for breath monitoring. The authors in [17] [19] leverage breath rate estimation for detecting sleep apnea. In these works the subcarrier with higher variance [17] or periodicity level [19] are used to estimate the breath rate. However, these systems can only detect breathing when the monitored person is stationary, i.e. either sleeping or sitting. In order to

realise a system that can monitoring breathing in an *in-situ* setting while the person goes about their regular activities, it is necessary to develop methods that can separate the impact of other motions from that of breathing. This is particularly challenging since the chest contractions and expansions caused by breathing are very subdued actions and as such the perturbations introduced in the CSI data are usually overpowered by other motions undertaken by the subject. In this work we exploit the diversity of subcarriers and antenna pairs of WiFi RF signals and reveal that particular subcarriers are sensitive to the subtle chest motions. Our proposed WiCare system can identify breath rate when the monitored individual undertakes micro motions that involve movement of his head, hand and arms. This is an important step towards the ultimate goal of being able to monitor breathing in a completely uncontrolled environment.

# 3 BACKGROUND

## 3.1 Channel State Information

Most modern off-the-shelf WiFi devices support the IEEE 802.11n/ac standard and include multiple antennas for MIMO communications. These devices employ orthogonal frequency-division multiplexing (OFDM) at the PHY layer. OFDM divides the frequency band into multiple subcarriers and simultaneously transmits multiple symbols in parallel. The frequency response of OFDM subcarriers is monitored as Channel State Information (CSI) [35] by the WiFi NICs. Let $X_i^p$ and $Y_i^p$ represent the transmitted and received symbols for subcarrier $i$ and antenna pair $p$. Let $H_i^p$ denote the wireless channel's CSI at any time instant. Then,

$$Y_i^p = H_i^p \times X_i^p \quad i \in [1, C] \quad p \in [1, N_t \times N_r] \tag{1}$$

$N_t$ and $N_r$ represent the number of transmit and receive antennas, which constitutes a $N_t \times N_r$ MIMO system. The hardware used in our experiments uses 3 transmit and receive antennas, i.e. $N_t = N_r = 3$. $H_i^p$ is a complex value $H_i^p = \|H_i^p\| e^{i \cdot \theta}$ where, $\theta$ is the phase and $\|H_i^p\|$ simplified as $H_i^p$ denotes the amplitude. CSI amplitude depict power fading of channels and capture the effects of multiple wireless phenomena such as absorption fading, multipath, destructive and constructive interference. The Intel 5300 NIC [13] is used in our experiments and provides information about 30 (i.e. C=30) OFDM subcarriers of 802.11n between each antenna pair. Thus the dimension of the CSI time series is $30 \times N_t \times N_r$.

## 3.2 Propagation Model

To monitor breathing in a natural setting where the observed individual undertakes certain actions (e.g. the micro motions outlined earlier), it is essential to gain insights into how breathing and micro motions affect the wireless signals and consequently the CSI data. In a typical indoor setting (such as Fig. 1), the WiFi signals are affected by the existence of objects in the surroundings such as furniture, walls, etc. and the body of the person being monitored. Copies of the transmitted signals reflected or diffracted by the surface of the various objects (chest, hand, furniture, walls, etc.) will arrive at the receivers along multiple propagation paths, which is called multipath effect. In order to characterise the multipath effect we consider a typical setting as shown in Fig. 2. For simplicity, the figure depicts the different propagation paths between a single

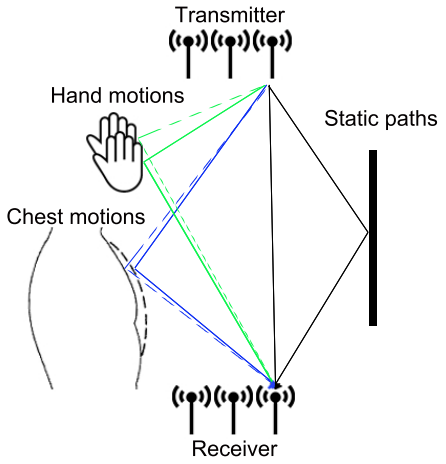


**Figure 2: Multipath propagation caused by static and dynamic objects.**

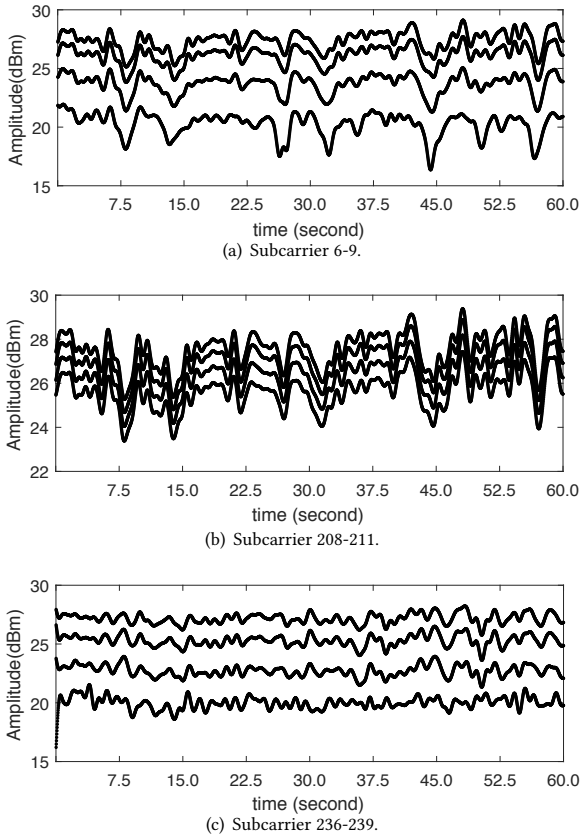


**Figure 3: CSI data for subcarrier 6-9, 208-211 and 236-239. In subcarriers 6-9, hand motions dominate chest motions. In subcarriers 208-211, two motions are both present. Subcarriers 236-239 mostly pronounce chest motions.**

transmit-receive antenna pair. These can be grouped into static paths and dynamic paths. The static paths $H_s$ include the direct path from the transmitter to receiver and reflected paths from stationary objects such as furniture, walls, etc. The dynamic paths $H_d$ are caused by the moving objects i.e., the chest (contraction and expansion caused by breathing) and hand (due to micro-motions). The CSI data $H_i^p$ (see Eg. (1)) is represented as follow [32],

$$H_i^p = H_s + H_d = H_s + \alpha A_1 e^{j(-2\pi f t_1)} + \beta A_2 e^{j(-2\pi f t_2)} \quad (2)$$

where $A_1$, $t_1$, and $e^{j(-2\pi f t_1)}$ and $A_2$, $t_2$, and $e^{j(-2\pi f t_2)}$ represent the amplitude, propagation delay and phase shift for the paths reflected off the chest and hand, respectively. $f$ is the frequency of the subcarrier $H_i^p$. Note that, $H_s$ is constant while $H_d$ is varied because the motion of the dynamic objects changes the path lengths and corresponding propagation delays $t_1$ and $t_2$ which contribute to the perturbations of CSI data. The coefficients $\alpha$ and $\beta$ represent the sensitiveness of the antenna pairs to the chest and hand motions, respectively. Since, the spatial distance from chest/hand to the $3 \times 3$ ($N_t \times N_r$) antenna pairs are not equal, $\alpha$ and $\beta$ are different.

We employ the Two-Ray propagation model [23] which is typically used for analysing multipath effects, to study the cumulative effect of the different paths outlined above at the receiver. Expanding the exponential terms in Eg. (2), the magnitude of the received signal can be represented as, [9]:

$$\|H_i^p\| = \sqrt{\alpha^2 A_1^2 + \beta^2 A_2^2 + 2\alpha\beta A_1 A_2 \cos[-2\pi f(t_2 - t_1)]} \quad (3)$$

Note that, $\|H_i^p\|$ depends on the subcarrier frequency $f$ because radio propagation is frequency-dependent. If, for example, the difference in the length of the two multi-paths (i.e., paths 1 and 2) equals to an odd number of half-wavelengths, then the cosine will be equal to -1 and the signal received over the two paths will combine destructively. Alternatively, if the path lengths differ by an even number of half-wavelengths, then the cosine will be equal to +1 and the signals will combine constructively. Accounting for the differences in the sensitivity coefficients, $\alpha$ and $\beta$, specific subcarriers may either uniquely contain the effect of breathing or micro motions or a combination of the two. Fig. 3 plots the CSI measurements of different frequencies (WiFi subcarriers) after applying a Butterworth 1 Hz low pass filter. The data is collected while an individual is performing a certain micro-motion. The specific details of the experimental setup are outlined in Section 5. Fig. 3(a) shows the sub-carriers where the hand motions dominate the chest motion. Fig. 3(b) shows the sub-carriers where the two motions are both present with approximate similar intensity. Finally, Fig. 3(c) illustrates sub-carriers in which breath dominates. The above analysis thus shows that certain subcarriers carry strong imprints of the breathing motions and are thus likely to be useful for measuring the breath rate. However, precisely identifying these subcarriers is challenging. This is because it is difficult to accurately measure the sensitivity coefficients and the precise manner in which the two motion signals will affect each other in each subcarrier. Moreover, the specific subcarriers relevant for breathing can change depending on the micro motion being performed. The insights gained here help to guide the design of the WiCare system discussed in the next section.

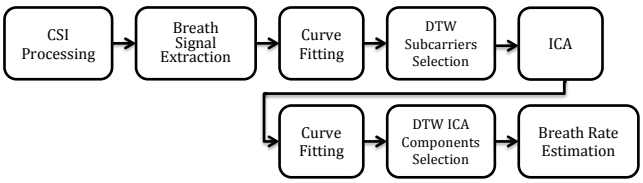


**Figure 4: Overview of WiCare.**

# 4 WICARE

## 4.1 Overview of WiCare

Fig. 1 depicts the typical operational scenario for the WiCare system. WiCare consists of a transmitter that periodically transmits packets to a receiver. The receiver records the CSI data for each received packet. As outlined in Section 1, the ultimate goal is to achieve *in-situ* breath monitoring of an individual while they go about their typical activities in their home or office. However, such an uncontrolled environment introduces significant challenges. The chest motions that result from breathing are very subtle as compared to the motions of other body parts (torso, limbs, etc.). The perturbations caused by the latter in the WiFi signals are significantly stronger than those by the former, which in turn makes it very challenging to accurately isolate the breathing signals. To make the problem more tractable, in this work, we assume that the monitored individual can perform certain micro motions which involve movement of their head, hand and arm while being seated. Some examples include reading, writing, using a mobile device, etc. A detailed list of the activities considered is in Table 1. We exclude all other intense motions that include movement of the torso and/or legs. We will show that accurate detection of breathing rate is considerably challenging in this seemingly simplified setting. WiCare represents a first and important step towards realising *in-situ* breath monitoring in natural settings.

In Section 3.2, we used a two ray propagation model to analyse multipath effects caused by chest and micro motions. It showed that some subcarriers are potentially more sensitive to chest motions due to the frequency and spatial diversity. Fig. 4 depicts the basic building blocks of WiCare which aims to identify these sensitive subcarriers and isolate breath signals. In the first instance, WiCare eliminates the effects of environmental noise which can be largely attributed to multi-path effects resulting from the WiFi signals reflected from other objects (e.g. furniture, walls, etc.) in the surrounding space which is discussed in Section 4.2. In Section 4.3, we transform the empirically collected CSI data to the frequency domain and illustrate that the impact of the breathing motions are restricted to a specific narrow range of frequencies. We also observe that the micro motions manifest their impact over a wider range of frequencies. WiCare employs Continuous Wavelet Transformation (CWT) to extract signals from the range of frequencies that captures the majority of the breathing signals. However, note that these frequencies also contain an imprint of the micro motions.

The insights gained from Section 3.2 suggest that subcarriers of antenna pairs are not equally sensitive to breathing. WiCare models breathing as a sinusoidal signal and uses curve fitting to compare the time series of each subcarrier against the template

(see Section Section 4.4.1). Dynamic Time Warping (DTW) is used to select the subcarriers that are most likely to capture breathing motions (see Section Section 4.4.2). Even though the selected subcarriers contain the breathing signals as the dominant component, they will also contain some impact of the micro motions. WiCare employs Independent Component Analysis (ICA) to separate the signals resulting from these two components. While we expect the breathing signal to be the dominant component, this is not always the case as some micro motions (e.g. use a tablet in Fig. 6(b)) are also manifested as strong signals in the same subcarriers. Thus, we use the same approach outlined above, i.e., curve fitting and DTW, to determine which component best matches the breath sinusoid. These steps are outlined in Section 4.4.3. Once the breath signal is isolated, a peak detection method is employed to calculate the breathing rate (Section 4.4.4).

## 4.2 CSI Preprocessing

It is well-known that physical objects in our surroundings (e.g. walls, ceiling, floor, furniture, etc.) introduce significant multi-path effects on radio transmissions. In the typical setting depicted in Fig.1, the reflected signals would arrive at the receiver with a significantly longer delay than the signals propagating along the direct path between the sender and receiver and also those reflected of the person's body (chest, arms, etc.) which are much closer to the receiver as compared to the surrounding objects. Removing these delayed components will mitigate the impact of the surrounding environment on the system. In achieve this, we transform the CSI data $H_i^p$ (see Eg. (1)) measured in frequency domain to the time domain by applying Inverse Fast Fourier Transform (IFFT). The time-domain profile of multipath communication channels is described as follow,

$$h_i^p(t) = \sum_{m=1}^{N} a_m(t)\delta(t - t_m) \tag{4}$$

where $N$ denotes the total number of multipath signals and $a_m(t)$ and $t_m$ represent the path gain and propagation delay of the $m_{th}$ path, respectively. $\delta(t)$ is the Dirac delta function. Prior research [15] has demonstrated that for indoor environments, the maximum propagation delay incurred by a reflected path is 500ns. Thus we remove the delay components in $h_i^p(t)$ that are larger than 500ns. Following, this the filtered signal is transformed back to the frequency domain using FFT. After filtering out environment impacts, we use a sliding window to identify breath in time series of the CSI data. The window size $T$ affects the breathing rate estimation accuracy which is evaluated in Section 5.2. In the next sub-section we outline the methods outlined for isolating the breathing signals from the more dominant signals induced by the micro-motions.

## 4.3 Breath Signal Extraction

In this section we analyse the filtered CSI data to understand how breath and the accompanying micro motion uniquely impact the CSI signals. The insights gained are used to derive a methodology for separating the breathing signals from accompanying micro motions. Breathing results in a repetitive up and down motion of the chest caused by inhalation and exhalation. As such, the perturbations induced by breathing in the CSI signals can be represented as a sinusoidal wave. Thus. if the CSI data purely contains the impact of breathing, then when it is transformed to the frequency domain, there will be one dominant frequency component corresponding to the respiration rate, where most of the energy will be concentrated. Prior research [19] has used this logic to isolate the signals corresponding to this frequency and measure the breathing rate. However, when the monitored subject performs micro motions, the resulting perturbations shadow the breath motions since these activities are typically more intense than the subtle chest motions associated with breathing. As a result, the prior approach [19] that relies on locating the dominant frequency is no longer useful for isolating the breathing signals. To gain insights into the coexistence of these two activities (i.e. micro motions and breathing), we compare the CSI data collected when the monitored individual is undertaking micro motions to when he is still (i.e. solely breathing). Details about how the experiments were conducted can be found in Section 5.

We employ Continuous Wavelet Transformation (CWT) and Morlet wavelet to transform the CSI data into the wavelet domain. CWT allows us to investigate the time varying frequency components in the signal. Breath motions are typically observed in the low-frequency range. Hence, we use wavelet transform as it offers higher resolution in the low frequency components. Fig. 5 illustrates the energy distribution of the CSI data after applying wavelet transform for the following 3 scenarios: - (a) when the person is still (and thus only breathing), (b) when the person is using his tablet and (c) when the person is drinking water. We only illustrate two micro-motions as representative examples. The subsequent observations are consistent for all micro motions considered in our experiments. In Fig. 5(a) we observe most of the energy is concentrated in the following three frequency ranges: (i) 0.028 Hz to 0.054 Hz, (ii) 0.295 Hz to 0.414 Hz and (iii) 23.873 Hz. Since the monitored individuals sit still in first scenario, the energy of the signal is largely concentrated in the second frequency range which corresponds to the breathing frequency of a normal adult. The energy in extreme low and high frequencies are largely base signals and environment noise respectively. In contrast, observe that when micro-motions are combined with breathing (Fig. 5(b) and Fig. 5(c)), the energy is spread across a wider frequency range and the subtle breath motions are not as easily isolated. Also observe that while in both these instances there is still some energy concentrated in the range from 0.295 Hz to 0.414 Hz, it is much lower than when the person is still and breathing. To isolate breathing signals, we employ the inverse wavelet transform to extract signals from 0.295 Hz to 0.414 Hz where the breathing signal is most likely to be concentrated. Next, we perform data normalisation to scale CSI data between 0 to 1. Data normalisation averages the transmission power of every subcarrier and highlights the shape of the isolated signals. While, majority of breathing motions are preserved, the extracted CSI data will also contain some influence of the accompanying micro motions. Recall from Section 3.2, that certain specific subcarriers are more likely to contain breathing signals than others. Next, we focus on selecting these informative subcarriers to detect the breathing rate.

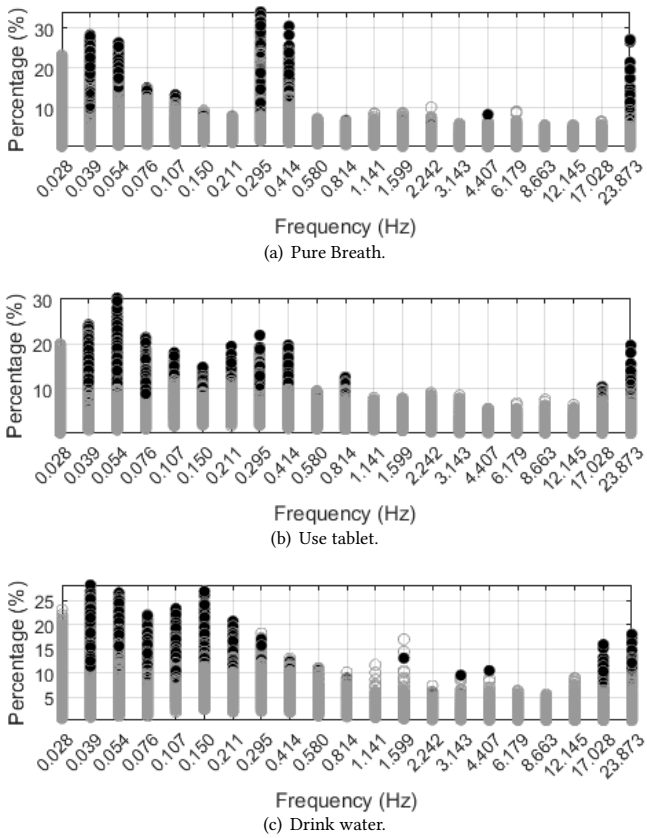


(a) Pure Breath.

(b) Use tablet.

(c) Drink water.

**Figure 5: Energy distribution when a person is still compared to when the person undertakes two different micro motions.**

## 4.4 Breath Identification

Our goal herein is to identify breathing signals from the transformed CSI data as outlined Section 4.3 and accurately estimate breath rate. As outlined in Section 3.2, a distinct set subcarriers are more sensitive to breathing and micro motions. Moreover, the specific subcarriers in each group are not known a priori. WiCare employs Curve Fitting and Dynamic Time Warping for adaptively selecting the subcarriers that correspond to breathing as outlined in Section 4.4.1 and Section 4.4.2. The selected subcarriers may still reflect the impact of micro motions. WiCare uses Independent Component Analysis as outlined in Section 4.4.3 to further isolate breathing signals. A peak detection method is used to estimate breathing rate as discussed in Section 4.4.4.

*4.4.1 Curve Fitting.* When a person breathes, his chest expands and contracts in a consistent and periodic manner. While these motions are subtle, they are manifested as a periodic pattern in the CSI data. Thus we model the impact of breathing on the CSI subcarriers as a sinusoidal wave. This assumption is consistent with prior work [19]. Specifically, we represent the impact of breathing on subcarrier $r(t)$ as,

$$s(t) = A\cos(2\pi f(t) + \phi) + \epsilon \tag{5}$$

where $A, f, \phi, \epsilon, t$ stand for amplitude, frequency, phase, shift of the sinusoidal wave and time, respectively.

For identifying the sinusoidal breath signals, WiCare use the interior-point approach [10] which is a non-linear optimizaiton technique for solving approximate constrained minimization problems presented as the following:

$$\begin{aligned} \text{minimize} \quad & \sum (s(t) - r(t))^2 \\ \text{subject to} \quad & A_1 \le A \le A_2, \\ & f_1 \le f \le f_2, \\ & -\pi \le \phi \le \pi, \\ & 0 \le \epsilon \le 1. \end{aligned} \tag{6}$$

The set of constraints define the bounds of the variables in Eq. (5). The amplitude of the identified sinusoidal breath signal is within $[A_1, A_2]$. As mentioned in Section 4.3 CSI data is normalised between 0 to 1. We heuristically set $A_1$ to 0.3 and $A_2$ to 1 for reliability. Human respiration can vary between 10 to 30 beats per minute depending on the age of the person [12]. Consequently, the frequency bounds, f1 and f2 are set to 2Hz and 6Hz. The optimisation is a typical curve fitting method for generating the ideal sinusoidal breathing signals. Fig. 6 shows the fitted sinusoid waves and the original CSI sequence in two subcarriers collected when the monitored individual is undertaking a particular micro motion (i.e. use tablet). Observe from the top figure that the breathing sinusoid has high similarity with the original CSI data, which suggests that this particular subcarrier is significantly influenced by breath motions and to a lesser extent by the accompanying micro motions. In contrast, one can readily observe from the bottom graph that there is significant dissimilarity between the sinusoid and the original CSI data for the other subcarrier. This suggests that this particular subcarrier is more significantly influenced by the micro motion rather than breathing. Thus, WiCare uses the goodness of the curve fit to determine which subcarriers are most influenced by breathing. The goodness of the fit is measured using Dynamic Time Warping (DTW) as outlined in the following.

*4.4.2 Dynamic Time Warping based Subcarrier Selection.* Normally, there are subtle changes in the breathing pattern of an individual. Inspiratory and expiratory duration and tidal volume of an individual varies in every breath [7], particularly so when they are carrying out some actions such as the micro motions under consideration. As such the actual breathing signals may not have constant amplitude and periodicity and may thus differ slightly from the sinusoidal template. DTW [31] [25] is known to be resilient to such variations. DTW seeks an alignment by matching each point of the first signal to one or more points of the second signal, thus minimising the distance between signals. We use the minimum distance to measure the similarity between time series of CSI and sinusoid. An experiment involving hand micro motions is conducted and the Fig. 7(a) shows the distances of 30 subcarriers of one TX-RX antenna pair. Observe that only a few subcarriers (subcarriers 6 to 10) exhibit a small distance (and thus similarity) to the sinusoid. Fig. 7(b) illustrates the CDF of the distance for all 270 subcarriers. It is evident that a vast majority of the subcarriers are dissimilar to the sinusoid. However, there are a few selected subcarriers that are influenced in a significant way by breathing. WiCare selects $S$

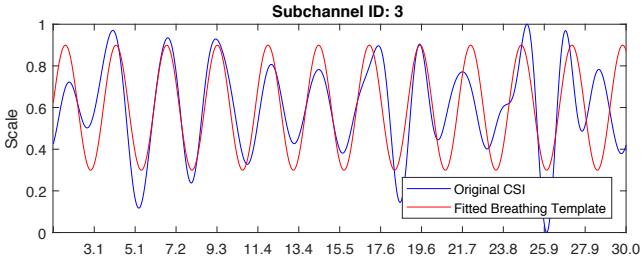


(a) subcarrier #3 Curve fitting.

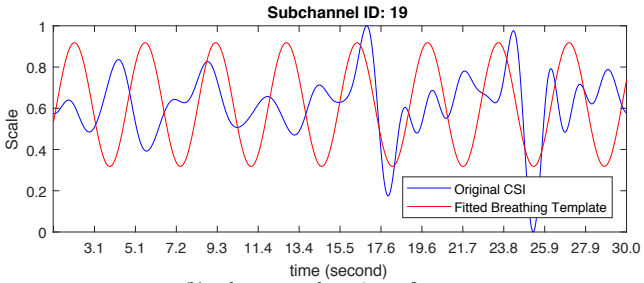


(b) subcarrier and #19 Curve fitting.

**Figure 6: The original signal and fitted sinusoidal breathing signals in two subcarriers. The CSI dataset is the mixture of breath and micro motions.**

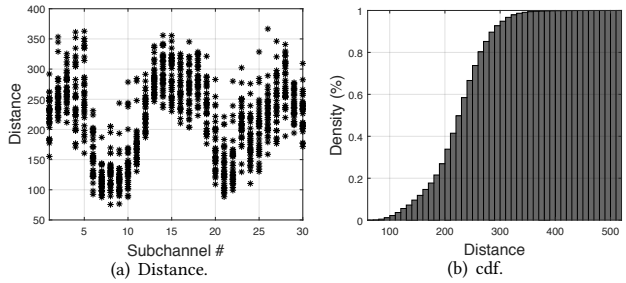


(a) Distance. (b) cdf.

**Figure 7: The distance between CSI data and fitted sinusoidal signals in 30 subcarriers of one TX-RX antenna pair is shown in Figure (a). The cumulative density function of the distance for all 270 subcarriers is shown in Figure (b).**

subcarriers which have the lowest distance for further processing. In Section 5.3 we evaluate the impact of selecting different values of *S*. While the selected subcarriers largely contain breathing signals, they may still reflect the influence of micro motions. In the next subsection, we outline how the breathing signal is precisely isolated.

*4.4.3 Independent Component Analysis.* The perturbation of CSI data in the selected subcarriers have two main sources, i.e. breathing and micro-motions, of which the former is most dominant. WiCare uses Independent Component Analysis (ICA) to precisely isolate the breathing signals in the selected subcarriers. ICA is one of the most popular blind source separation methods, which aims to separate the mixed signals into a set of independent components given very little information (or no prior information) about the source signals. It has been successfully applied in numerous domains such as biomedical signal processing [27], gait analysis [34] and speech separation [26]. Let *CSI(t)* represent the CSI data for the selected subcarriers in Section 4.4.2. Since, these CSI signals are a mixture of signals from breathing and micro motions, they can be represented as follows,

$$CSI(t) = A \cdot CSI_{source}(t) \tag{7}$$

where $A$ is the mixing matrix and $CSI_{source}(t)$ represents independent sources. Our aim is to find an unmixing matrix $W (W = A^{-1})$, so that we can calculate the estimated source signal $\tilde{CSI}_{source}(t)$ as follows,

$$\tilde{CSI}_{source}(t) = W \cdot CSI(t) = W \cdot A \cdot CSI_{source}(t) \tag{8}$$

In this paper, we use FastICA, a fast and efficient fixed-point algorithm to solve the ICA model in Eq. 8, i.e., to estimate $W$. FastICA has been found to be 10-100 times faster than conventional gradient descent methods for ICA [14]. After obtaining $W$, we can get the estimated sources $\tilde{CSI}_{source}(t)$ by Eq. 8. Fig. 8(a) shows CSI data of the subcarrier that is closest to the sinusoidal breathing signal. Fig. 8(b) and Fig. 8(c) presents the measured CSI after source separation. The independent component in Fig. 8(b) corresponds to the pure breathing signal which was originally mixed with the micro motion signal. Next, we again use curve fitting and DTW-based subcarrier selection outlined in Section 4.4.1 and Section 4.4.2 to select the component that best matches the breath sinusoid. In particular, $\tilde{CSI}_{source}(t)$ are applied to Eq. 6 as $r(t)$ and DTW helps to select the independent component with the minimum distance to sinusoid as the isolated breath signal.

*4.4.4 Breath Rate Estimation.* After obtaining the relatively isolated CSI data that captures pure breathing, we apply peak detection to estimate the breathing rate. A moving window of ten samples is used to avoid incorrect identification of peaks. Fig. 9 presents the peak detection applied on the isolated breath signal. The number of peaks $P$ divided by the time duration $T$ of the CSI sequence will be the breath rate $f = P/T(s) * 60$ breath per minute (bpm). The window size $T$ affects the precision of the estimated breath rate which will be evaluated in Section 5.2.

## 5 EVALUATION

In this section we present a comprehensive evaluation of the WiCare system. Section 5.1 outlines the experimental setup and scenario. Section 5.2 presents results for different window sizes $T$ mentioned in Section 4.2. Section 5.3 evaluates the impact of using different $S$ subcarriers on the accuracy mentioned in Section 4.4.2. Finally, Section 5.4 evaluates accuracy of estimating the breathing rate for WiCare when the monitored subjects undertake nine different micro motions. A comparison with the state-of-the-art benchmark is also presented.

### 5.1 Experiment Setup

We implemented a prototype of WiCare using off-the-shelf WiFi devices. We specifically used two identical HP 8530p laptop equiped with an Intel WiFi link 5300 802.11n chipset. One laptop acts as the transmitter and the other one acts as the receiver. We installed

**Table 1: Related works in different activities for breath monitoring.**

| Activities | Static | Type | Slide | Phone | Write | Drink | Head | Read | Remote |
|---|---|---|---|---|---|---|---|---|---|
| WiCare | ✓ | ✓ | ✓ | ✓ | ✓ | ✓ | ✓ | ✓ | ✓ |
| Others | ✓ | ✓ | ✗ | ✗ | ✗ | ✗ | ✗ | ✗ | ✗ |

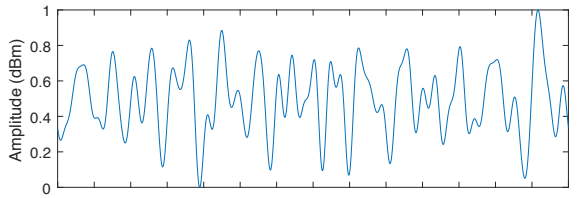

(a) The closest subcarrier.

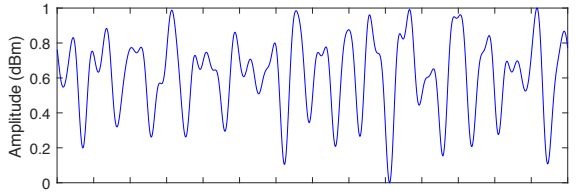

(b) One ICA component.

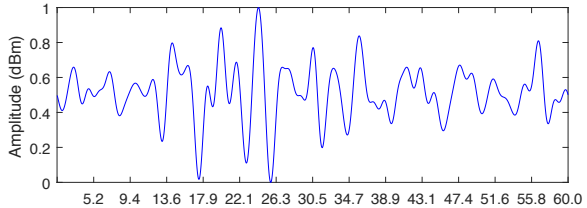

(c) Another ICA component.

**Figure 8: The independent components of selected subcarriers. The figure (a) shows one CSI sequence of the subcarrier that has the minimum distance. The figure (b)(c) show the two independent components. The component in the figure (b) is expected to be selected as the true breath profile for the breath rate calculation**

Ubuntu 10.14 with modified Intel NIC driver [13] on both HP laptops. We set the driver to operate in injection mode, wherein packets are transmitted using a pre-defined modulation and coding scheme to ensure stable operation. Both laptops have 3 antennas (i.e. $N_t = 3$ and $N_r = 3$), which results in 30 (subcarriers) $\times 3 \times 3 = 270$ time series data streams in the CSI data. The two devices were placed on a table approximately one meter apart from each other and the distance from the monitored individual to either laptop was approximately 0.5 meter. The entire WiCare system depicted in Fig. 4 was implemented in the laptop operating as the receiver.

The centre frequency of the WiFi channel is set to 5.51Ghz and the bandwidth is 40 MHz. The transmitter is programmed to broadcast packets every 20ms (50Hz) to the receiver. The CSI data is

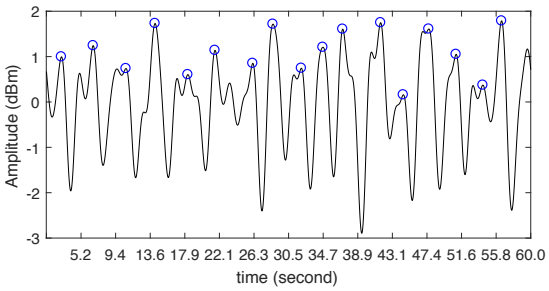


**Figure 9: Breath Rate Estimation**

recorded at the receiver and analyzed as per the processes outlined in Fig. 4 (and Section 4.1). The ground truth for the breathing rate is measured by mounting a Genuino 101 board [1] equipped with a 3-axis accelerometer sensor to the chest of the monitored individual. The peak detection method outlined in Section 4.4.4 is also applied to estimate breath rate from the accelerometer data.

We asked the monitored individuals to perform the following 9 micro-motions while sitting: sit still, type on a keyboard, use a tablet, play a game on a phone, write with a pen, drink a glass of water, nod their head, read a book, use TV remote controller (also listed in Table 1). Sitting still and typing on a keyboard involve minimal motion. When a person is using a tablet, the primary action is created by the hand used to interact with the tablet. Nodding involves movement of the head. The remaining actions, i.e. drinking water, reading a book, playing a game on a phone and using the TV remote typically involves the movement of one or both hands, arm and the head. These are typical activities performed by an individual while sitting and relaxing in their home [20]. Prior research [7] shows human beings have diversified breathing rates therefore we recruited 5 participants and asked each participant to perform each activity repeatedly for 5 minutes. The experiments were conducted in an indoor environment where the existing WiFi network used for Internet access was operational for the entire time. We also implemented a system based on [17] as a benchmark, which we refer to as TrackVitalSign in the rest of this section. This system was designed to monitor the breathing rate of an individual while they are sleeping. We use this in our comparison to show that this approach is not effective when the monitored individual performs certain actions.

We use the accuracy of breathing rate estimation as the evaluation metric. Let $f_{estimated}$ refer to the estimated breathing rate by the system being evaluated (i.e. WiCare or TrackVitalSign) and let $f_{true}$ refer to the ground truth as measured by the chest mounted sensor. Then we define the breathing rate is correctly estimated if $f_{estimated} \in [0.9 f_{true}, 1.1 f_{true}]$, which is similar to the approach adopted in [19]. The results presented in the graphs are average results. The standard deviation is also illustrated.

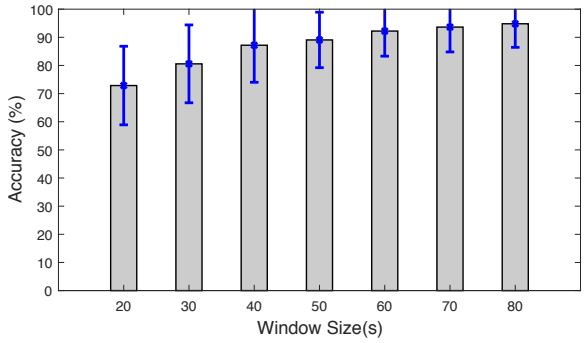


**Figure 10: Impact of the various window sizes**

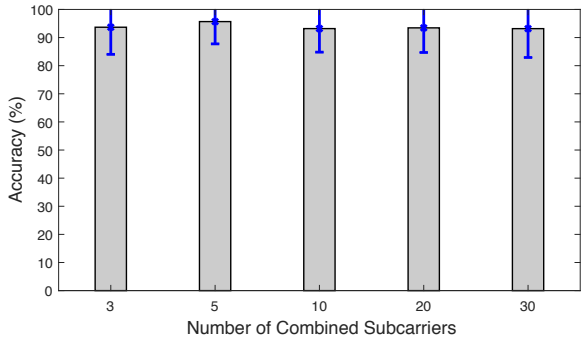


**Figure 11: Impact of the number of combined subcarriers**

## 5.2 Effect of window size

We first evaluate the impact of changing the window size $T$ of time series of CSI data mentioned in Section 4.2. For this evaluation we combine the data for all 9 micro motions from all 5 participants. Fig. 10 shows the accuracy of the estimated breath rate for different window sizes (from 20s to 80s). We observe a longer window size tends to improve the estimation accuracy. However, a large window size also increases the system latency. As can be observed from Fig. 10, the improvement in accuracy beyond a window size of 60 seconds is very marginal. Thus, we choose to set $T$ to 60 seconds in the rest of the evaluations.

## 5.3 Effect of number of chosen subcarriers

Recall from Section 4.4.2, that WiCare selects a subset $S$ of the total subcarriers that best match the sinusoidal template of the breath signal. In this section, we study the impact of including different number of subcarriers (i.e. $S$) on the estimation accuracy. Fig. 11 illustrates that the average accuracy is over 90% for different number of subcarriers. However, we observe that the accuracy is highest and the variance is lowest for 5 subcarriers. Thus, in the rest of the evaluations we consider 5 subcarriers.

## 5.4 Breath rate estimation

Finally, we evaluate the accuracy of WiCare in estimating the breathing rate of an individual while they are performing certain micro motions. We have selected a diverse set of activities for our tests

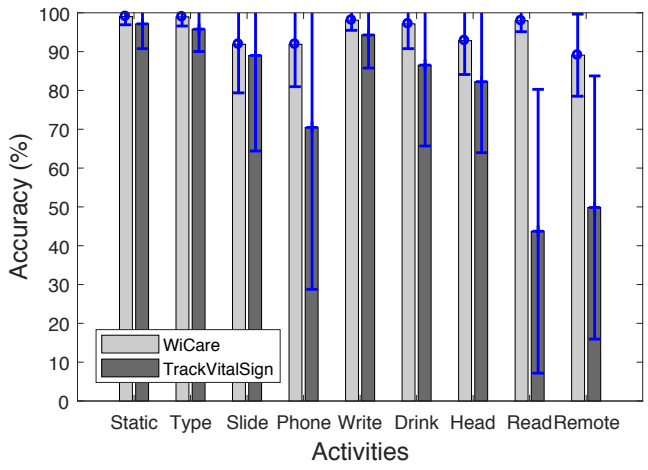


**Figure 12: Impact of 9 activities involving multiple body part motions.**

listed in Table 1. Fig. 12 presents the results for the 9 different micro motions. WiCare consistently achieves an average accuracy of over 90%. In contrast, TrackVitalSign can only achieve comparable performance for the static and typing micro-motions. The accuracy drops significantly for most other motions, the accuracy when the person is reading a book is only 10%. Fig. 13 presents the cumulative distribution of the estimation errors across all activities. WiCare achieves an estimation error of lower than 2bpm error for the vast majority of experiments (80%). In contrast, TrackVitalSign can only achieve comparable performance for the static and typing micro-motions. In summary, WiCare can consistently and accurately estimate the breathing rate even when the person is undertaking a wide range of micro motions. This is an important step towards realising continuous and long-term breath monitoring of individuals in their natural environment.

# 6 CONCLUSION

Monitoring the respiration rate can contribute to early diagnosis of chronic respiratory diseases. In this paper, we presented a system called WiCare that is able to accurately estimate *in-situ* breathing rate in a natural setting where the individual can perform various micro motions. To distinguish breath from micro motions, WiCare exploits curve fitting and DTW to identify certain specific subcarriers that capture the bulk of the imprint of breathing motions because of multipath effect and frequency and spacial diversity of MIMO systems. Next, ICA is used to precisely isolate breathing signals and a peak detection method is used to estimate breathing rate. Extensive experiments demonstrate WiCare is able to accurately identify breathing from micro motions and estimate breathing rate with an average accuracy of over 90%. WiCare also outperforms the state-of-the-art breath rate estimation method by up to 80%.

# REFERENCES

[1] Genuino 101 board. https://www.arduino.cc/en/Main/ArduinoBoard101. Accessed: 2017-05-8.
[2] Hexoskin smart shirt. http://https://www.hexoskin.com/. Accessed: 2017-02-20.
[3] Mimo baby monitor. http://https://http://mimobaby.com//. Accessed: 2017-02-20.

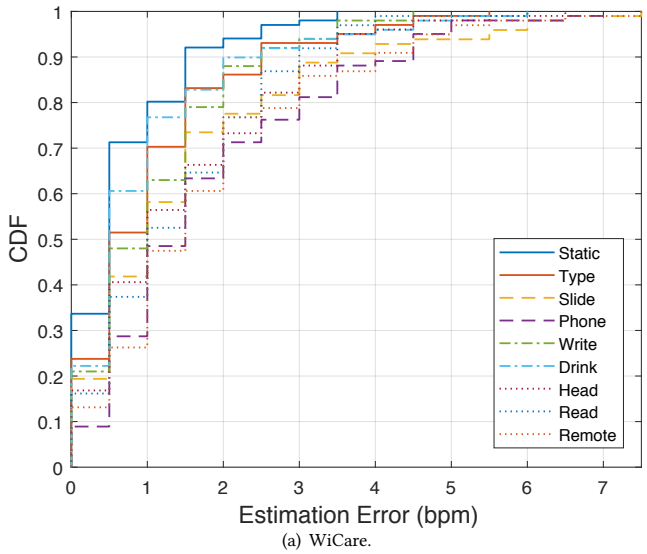


(a) WiCare.

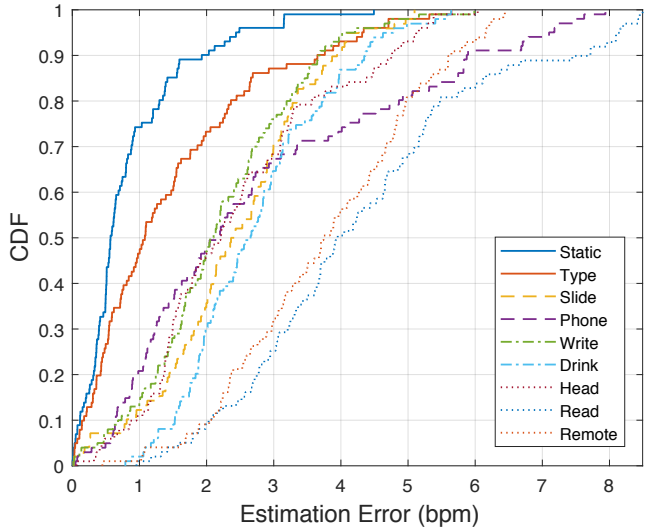


(b) TrackVitalSign.

**Figure 13: Cumulative distribution of breath rate estimation errors. The 9 activities are indicated by the colour and WiCare and TrackVitalSign are presented by Fig. 13(a) and Fig. 13(b).**


[4] Resmed air solutions masks. http://www.resmed.com/au/en/consumer/products/masks.html. Accessed: 2017-02-20.

[5] Who strategy for prevention and control of chronic respiratory diseases. http://www.who.int/respiratory/publications/crd_strategy/en/. Accessed: 2017-05-8.

[6] F. Adib et al. Smart homes that monitor breathing and heart rate. In *Proceedings of the 33rd Annual ACM Conference on Human Factors in Computing Systems*, pages 837–846. ACM, 2015.

[7] G. Benchetrit. Breathing pattern in humans: diversity and individuality. *Respiration physiology*, 122(2):123–129, 2000.

[8] P. Bernardi et al. Design, realization, and test of a uwb radar sensor for breath activity monitoring. *IEEE Sensors Journal*, 14(2):584–596, 2014.

[9] B. Black et al. *Introduction to wireless systems.* Prentice Hall Press, 2008.

[10] R. H. Byrd et al. A trust region method based on interior point techniques for nonlinear programming. *Mathematical Programming*, 89(1):149–185, 2000.

[11] A. D. Droitcour et al. Signal-to-noise ratio in doppler radar system for heart and respiratory rate measurements. *IEEE transactions on microwave theory and techniques*, 57(10):2498–2507, 2009.

[12] W. F. Ganong et al. *Review of medical physiology.* Appleton & Lange Norwalk, CT, 1995.

[13] D. Halperin et al. Tool release: Gathering 802.11 n traces with channel state information. *ACM SIGCOMM Computer Communication Review*, 41(1):53–53, 2011.

[14] A. Hyvärinen. Fast and robust fixed-point algorithms for independent component analysis. *IEEE Transactions on Neural Networks*, 10(3):626–634, 1999.

[15] Y. Jin et al. Indoor localization with channel impulse response based fingerprint and nonparametric regression. *IEEE Transactions on Wireless Communications*, 9(3), 2010.

[16] T. Karl et al. Human breath isoprene and its relation to blood cholesterol levels: new measurements and modeling. *Journal of Applied Physiology*, 91(2):762–770, 2001.

[17] J. Liu et al. Tracking vital signs during sleep leveraging off-the-shelf wifi. In *Proceedings of the 16th ACM International Symposium on Mobile Ad Hoc Networking and Computing*, pages 267–276. ACM, 2015.

[18] X. Liu et al. Wi-sleep: Contactless sleep monitoring via wifi signals. In *Real-Time Systems Symposium (RTSS)*, pages 346–355. IEEE, 2014.

[19] X. Liu et al. Contactless respiration monitoring via off-the-shelf wifi devices. *IEEE Transactions on Mobile Computing*, 15(10):2466–2479, 2016.

[20] B. Logan et al. A long-term evaluation of sensing modalities for activity recognition. In *International conference on Ubiquitous computing*, pages 483–500. Springer, 2007.

[21] N. Patwari et al. Monitoring breathing via signal strength in wireless networks. *IEEE Transactions on Mobile Computing*, 13(8):1774–1786, 2014.

[22] K. F. Rabe et al. Global strategy for the diagnosis, management, and prevention of chronic obstructive pulmonary disease: Gold executive summary. *American journal of respiratory and critical care medicine*, 176(6):532–555, 2007.

[23] T. S. Rappaport et al. *Wireless communications: principles and practice*, volume 2. Prentice Hall PTR New Jersey, 1996.

[24] R. Ravichandran et al. Wibreathe: Estimating respiration rate using wireless signals in natural settings in the home. In *Pervasive Computing and Communications (PerCom), 2015 IEEE International Conference on*, pages 131–139. IEEE, 2015.

[25] S. Salvador et al. Toward accurate dynamic time warping in linear time and space. *Intelligent Data Analysis*, 11(5):561–580, 2007.

[26] M. N. Schmidt et al. Single-channel speech separation using sparse non-negative matrix factorization. In *INTERSPEECH' 2006.*

[27] G. Srivastava et al. Ica-based procedures for removing ballistocardiogram artifacts from eeg data acquired in the mri scanner. *Neuroimage*, 24(1):50–60, 2005.

[28] L. Sun et al. Widraw: Enabling hands-free drawing in the air on commodity wifi devices. In *Proceedings of the 21st Annual International Conference on Mobile Computing and Networking*, pages 77–89. ACM, 2015.

[29] S. Tan et al. Wifinger: leveraging commodity wifi for fine-grained finger gesture recognition. In *Proceedings of the 17th ACM International Symposium on Mobile Ad Hoc Networking and Computing*, pages 201–210. ACM, 2016.

[30] H. Wang et al. Human respiration detection with commodity wifi devices: do user location and body orientation matter? In *Proceedings of the 2016 ACM International Joint Conference on Pervasive and Ubiquitous Computing*, pages 25–36. ACM, 2016.

[31] J. Wang et al. Dude, where's my card?: Rfid positioning that works with multipath and non-line of sight. *ACM SIGCOMM Computer Communication Review*, 43(4):51–62, 2013.

[32] W. Wang et al. Understanding and modeling of wifi signal based human activity recognition. In *Proceedings of the 21st Annual International Conference on Mobile Computing and Networking*, pages 65–76. ACM, 2015.

[33] B. Wei et al. Radio-based device-free activity recognition with radio frequency interference. In *International Conference on Information Processing in Sensor Networks*, pages 154–165. ACM, 2015.

[34] W. Xu et al. Walkie-talkie: Motion-assisted automatic key generation for secure on-body device communication. In *Proceedings of the 15th International Conference on Information Processing in Sensor Networks*, page 3. IEEE Press, 2016.

[35] Z. Yang et al. From rssi to csi: Indoor localization via channel response. *ACM Computing Surveys (CSUR)*, 46(2):25, 2013.

[36] J. Zhang et al. Wifi-id: Human identification using wifi signal. In *Distributed Computing in Sensor Systems (DCOSS), 2016 International Conference on*, pages 75–82. IEEE, 2016.

[37] D. Zito et al. Soc cmos uwb pulse radar sensor for contactless respiratory rate monitoring. *IEEE Transactions on Biomedical Circuits and Systems*, 5(6):503–510, 2011.